

Journal Name

Crossmark

ARTICLE TYPE

RECEIVED
dd Month yyyy
REVISED
dd Month yyyy

Multifractal Analysis of the Non-Hermitian Skin Effect: From Many-Body to Tree Models

Shu Hamanaka

Department of Physics, Kyoto University, Kyoto 606-8502, Japan

E-mail: hamanaka.shu.45p@st.kyoto-u.ac.jp**Keywords:** Multifractality, Non-Hermitian skin effect, Many-body systems, Quantum chaos**Abstract**

The non-Hermitian skin effect is an anomalous localization phenomenon induced by nonreciprocal dissipation and has attracted considerable attention in recent years both theoretically and experimentally. In this article, we review the multifractal aspects of the non-Hermitian skin effect. In particular, we discuss how the many-body skin effect exhibits multifractality in many-body Hilbert space, unlike the trivial Hilbert-space occupation of the single-particle skin effect on crystalline lattices. We further highlight that the many-body skin effect can coexist with random-matrix spectral statistics, in contrast to the multifractality associated with many-body localization, which typically accompanies the absence of ergodicity. We also introduce a solvable model on a Cayley tree as an effective description of the many-body Hilbert space, in which the multifractal dimensions can be obtained analytically. This review provides a unified perspective on multifractal structures in the non-Hermitian skin effect across single-particle, many-body, and tree models, and clarifies their distinctive relation to ergodicity in open quantum systems.

Contents

1	Introduction	2
2	Multifractal analysis	2
2.1	Definition of multifractal dimension	2
2.2	Multifractality in disordered systems	3
3	Single-particle skin effect	3
3.1	Hatano-Nelson model	3
3.2	Periodic boundary conditions	4
3.3	Open boundary conditions	4
4	Multifractality of many-body non-Hermitian skin effect	4
4.1	Model	5
4.2	Multifractal scaling	5
4.3	Spectral statistics	6
5	Tree geometry and analytic multifractality	7
5.1	Motivation	7
5.2	Model	8
5.3	Symmetric sector	8
5.4	Exact multifractal dimension	9
5.5	Multifractal dimensions of degenerate states	11
6	Conclusion and outlook	12

arXiv:2603.26185v1 [cond-mat.dis-nn] 27 Mar 2026

1 Introduction

Multifractality provides a universal description of the complex structures emerging in quantum states between localization and ergodicity [1]. In disordered systems, critical single-particle wave functions at the Anderson transition exhibit multifractal behavior [2–8], reflecting the complex distribution of quantum states. In the presence of interactions, many-body localized phases also display multifractal statistics due to the intricate structure of the many-body Hilbert space [9–12], often discussed in the context of the ETH–MBL transition. More recently, monitored quantum dynamics has also been shown to exhibit multifractal structures [13–15]. In this sense, multifractality provides a unifying language for characterizing complex intermediate structures of quantum states.

The non-Hermitian skin effect provides a distinct mechanism of localization [16]. In contrast to disorder-induced localization, the skin effect originates from nonreciprocal dissipation, leading to the anomalous accumulation of a macroscopic number of eigenstates at system boundaries. This phenomenon has attracted considerable attention due to its intimate relation to non-Hermitian topology [17–33] and its significant impact on open quantum dynamics [34–42]. Experimental realizations have also been reported in a variety of classical and quantum platforms [43–50].

While the skin effect in single-particle systems is now formulated in terms of non-Bloch band theory [51, 52] and point-gap topology [53, 54], its extension to interacting many-body systems has emerged as an active area of research, revealing rich phenomena arising from the interplay between many-body interactions and nonreciprocity [39, 41, 42, 55–72]. Representative examples include interaction-induced skin effects [65] and Mott skin effects [41]. Despite these developments, most previous studies have primarily focused on real-space particle number distributions, and a direct quantitative characterization of localization in the many-body Hilbert space has received comparatively less attention. In particular, the present article is guided by two closely related questions: *how do many-body skin modes occupy the exponentially large many-body Hilbert space, and which properties of the Hilbert-space structure govern this occupancy?* As we discuss below, the first question is addressed by the emergence of multifractality in many-body skin modes, while the second is illuminated by the analytically solvable tree model, where the interplay between hierarchical structure and nonreciprocity determines the occupation profile.

In this article, we review the multifractal aspects of the non-Hermitian skin effect across different settings, ranging from single-particle systems to many-body and tree models. Specifically, we discuss how the many-body skin effect is characterized by multifractality in many-body Hilbert space, unlike the trivial Hilbert-space occupation of conventional single-particle skin modes on crystalline lattices. We also highlight a key distinction from many-body localization: this multifractality can coexist with random-matrix spectral statistics. To shed light on the Hilbert-space structures underlying this multifractal behavior, we also discuss analytically solvable models on tree geometries, where the interplay between hierarchical structure and nonreciprocity allows exact derivations of multifractal dimensions. Taken together, this review provides a unified perspective on the skin effect from the viewpoint of multifractality, and clarifies its distinctive role in open quantum systems.

The rest of this paper is organized as follows. In Sec. 2, we briefly review the basics of multifractal analysis. In Sec. 3, we apply this analysis to single-particle skin effects and show that conventional skin modes on crystalline lattices do not exhibit multifractality, reflecting their trivial occupation of Hilbert space. In Sec. 4, we discuss how the many-body skin effect exhibits multifractality in many-body Hilbert space, and this multifractality can coexist with random-matrix spectral statistics. In Sec. 5, we introduce a solvable model on a Cayley tree and present analytical expressions for the multifractal dimensions. Section 6 is devoted to the summary and outlook.

2 Multifractal analysis

2.1 Definition of multifractal dimension

In this section, we briefly review the basic notions characterizing the multifractal scaling of the wave function. Let $|\psi\rangle$ be a normalized state with \mathcal{N} components in a chosen basis $\{|j\rangle\}_{j=1}^{\mathcal{N}}$:

$$|\psi\rangle = \sum_{j=1}^{\mathcal{N}} \psi_j |j\rangle. \quad (1)$$

The multifractal properties of $|\psi\rangle$ are encoded in the scaling behavior of its moments. Specifically, we consider the generalized inverse participation ratio [3]

$$I_q := \sum_{j=1}^{\mathcal{N}} |\psi_j|^{2q}, \quad (2)$$

which scale with system size as

$$I_q \propto \mathcal{N}^{-\tau_q}. \quad (3)$$

Here, τ_q is a nondecreasing ($\tau'_q \geq 0$) and convex ($\tau''_q \leq 0$) function satisfying $\tau_0 = -1$ and $\tau_1 = 0$. The multifractal dimensions D_q defined from the exponents τ_q ,

$$D_q := \frac{\tau_q}{q-1} = -\frac{1}{q-1} \frac{1}{\ln \mathcal{N}} \ln I_q, \quad (4)$$

which measure how broadly the wave function occupies the Hilbert space. Note that D_1 is defined by the derivative of τ_q at $q = 1$.

In what follows, we restrict ourselves to $q > 0$, for which the multifractal dimensions satisfy $0 \leq D_q \leq 1$. A fully extended state is characterized by $D_q = 1$, whereas a state confined to a finite portion of Hilbert space has $D_q = 0$. The intermediate regime $0 < D_q < 1$ corresponds to states that are extended but not fully delocalized. When D_q is independent of q in this range, the state is called *monofractal* and is described by a single effective dimension. By contrast, if D_q varies with q , the state is *multifractal*, indicating intricate distribution of wave-function amplitudes across Hilbert space. In such cases, no single exponent suffices, and an entire family of exponents is required to characterize the state.

The multifractal spectrum f_α , defined via the Legendre transformation [1],

$$f_\alpha := \alpha q - \tau_q \quad \text{at } q \text{ such that } \alpha = \frac{d\tau_q}{dq}, \quad (5)$$

describes the distribution of local scaling exponents α , in the sense that the number of components with $|\psi_j|^2 \sim \mathcal{N}^{-\alpha}$ scales as \mathcal{N}^{f_α} . For delocalized, localized, and more generally monofractal states, the spectrum collapses to a single point in the (α, f_α) plane: $(\alpha, f_\alpha) = (1, 1)$ for perfectly delocalized states, $(0, 0)$ for localized states, and (D, D) for monofractal states with a q -independent dimension $D_q = D$. By contrast, multifractality is characterized by a broadened spectrum with nonzero width, $\alpha_{\min} < \alpha < \alpha_{\max}$ where $f_\alpha > 0$, reflecting the coexistence of multiple scaling structures in the wave function. Equivalently, such a broadened spectrum corresponds to a q -dependent multifractal dimension D_q .

2.2 Multifractality in disordered systems

Representative examples of different multifractal behaviors are found in disordered systems. In the Anderson localized phase, wave functions are localized with $D_q = 0$, whereas in the delocalized phase they satisfy $D_q = 1$. Multifractality, $0 < D_q < 1$ with a q -dependent D_q , emerges at the Anderson transition [2–7] and in many-body localized phases [9–12, 73, 74]. Multifractality has also been observed in monitored quantum dynamics [13–15].

In the following, we investigate the multifractal dimensions associated with the non-Hermitian skin effect. In particular, we contrast conventional single-particle skin modes on crystalline lattices, which do not exhibit multifractality, with the many-body skin effect, where multifractal scaling emerges. We also introduce an analytically solvable model on a tree geometry, which provides further insight into the emergence of multifractal behavior from the underlying Hilbert space structure.

3 Single-particle skin effect

3.1 Hatano-Nelson model

The non-Hermitian skin effect is an anomalous localization phenomenon induced by nonreciprocal dissipation. The Hatano-Nelson model [75, 76] in the absence of disorder provides the simplest setting for illustrating this effect. The Hamiltonian is given by

$$H = \sum_j \left(t_R |j+1\rangle \langle j| + t_L |j\rangle \langle j+1| \right), \quad (6)$$

where $\{|j\rangle\}$ ($j = 1, \dots, L$) denotes the single-particle basis, and t_R (t_L) is the right (left) hopping amplitude. Below, we analyze the multifractal dimension of eigenstates under both periodic and open boundary conditions.

3.2 Periodic boundary conditions

Under periodic boundary conditions, the right eigenstates are plane waves

$$\psi_j^{(n)} = \frac{1}{\sqrt{L}} e^{ik_n j}, \quad (7)$$

with $k_n = 2\pi n/L$ ($n = 0, 1, \dots, L-1$). Then we can directly compute multifractal dimensions as

$$D_q = -\frac{1}{q-1} \frac{1}{\ln L} \ln \left(\sum_{j=1}^L \left| \frac{e^{ik_n j}}{\sqrt{L}} \right|^{2q} \right) = 1 \quad (8)$$

Hence, the multifractal dimension is unity, corresponding to a delocalized state.

3.3 Open boundary conditions

Under open boundary conditions, the right eigenstates take the form

$$\psi_j^{(n)} \propto \beta^j \sin(k_n j), \quad \beta := \sqrt{\frac{t_R}{t_L}}, \quad (9)$$

with $k_n = \pi n/(L+1)$ ($n = 1, \dots, L$) (see Ref. [51]). These eigenstates localize at the right (left) edge for $\beta > 1$ ($\beta < 1$), giving rise to the non-Hermitian skin effect. For analytical simplicity, we approximate the eigenstates as

$$\psi_j^{(n)} \simeq \frac{1}{\sqrt{N}} (\beta e^{ik_n})^j, \quad (10)$$

with the normalization constant

$$N = \sum_{j=1}^L \beta^{2j} = \frac{\beta^2(\beta^{2L} - 1)}{\beta^2 - 1}. \quad (11)$$

This approximation is consistent with the non-Bloch band theory [16, 51] and captures the essential nature of the skin effect. Then we can directly evaluate the multifractal dimensions as

$$\begin{aligned} D_q &\simeq -\frac{1}{q-1} \frac{1}{\ln L} \ln \left(\sum_{i=1}^L \left| \frac{(\beta e^{ik_n})^i}{\sqrt{N}} \right|^{2q} \right) = -\frac{1}{q-1} \frac{1}{\ln L} \ln \left(\left(\frac{\beta^2 - 1}{\beta^2(\beta^{2L} - 1)} \right)^q \frac{\beta^{2q}(\beta^{2qL} - 1)}{\beta^{2q} - 1} \right) \\ &\simeq -\frac{1}{q-1} \frac{1}{\ln L} \ln \left(\frac{(\beta^2 - 1)^q}{\beta^{2q} - 1} \right) \rightarrow 0, \end{aligned} \quad (12)$$

where we have taken the limit $L \rightarrow \infty$ with $\beta > 1$. Hence, the multifractal dimension vanishes, corresponding to the localized state.

Beyond one dimension, conventional crystalline skin modes are typically localized or, at most, monofractal rather than multifractal. For a state on a d -dimensional lattice that is exponentially localized along $d-n$ directions but extended along the remaining n directions, one finds $D_q = n/d$, which is independent of q . Thus, skin effects in higher dimensions, including higher-order skin effect [77, 78] exhibit only q -independent monofractal scaling rather than multifractality.

4 Multifractality of many-body non-Hermitian skin effect

In the previous section, we found that single-particle skin modes are perfectly localized and therefore have vanishing multifractal dimensions. We now turn to the many-body skin effect, where multifractal behavior emerges [67]. We first introduce the model and then examine its multifractal scaling. We also discuss how such multifractal behavior can coexist with random-matrix spectral statistics (Table 1).

Table 1: Spectral statistics and multifractality for various quantum phases of matter.

Quantum phase	Spectral statistics	Multifractality
Thermalization	Random matrix	Ergodic ($D_q = 1$)
Many-body localization	Poisson	Multifractal ($0 < D_q < 1$)
Non-Hermitian skin effect	Random matrix	Multifractal ($0 < D_q < 1$)

4.1 Model

To investigate the generic properties of the many-body non-Hermitian skin effect that do not rely on special integrable structures or model-specific details, we consider the following nonintegrable non-Hermitian spin chain:

$$H = \sum_{i=1}^L \left[\frac{t}{2} \left((1 + \gamma) \sigma_i^- \sigma_{i+1}^+ + (1 - \gamma) \sigma_i^+ \sigma_{i+1}^- \right) + J \sigma_i^z \sigma_{i+1}^z + g \sigma_i^x + h \sigma_i^y \right], \quad (13)$$

where $t, \gamma, J, g, h \in \mathbb{R}$. Here, $\sigma_i^x, \sigma_i^y,$ and σ_i^z denote Pauli matrices at site i , and $\sigma_i^\pm = \sigma_i^x \pm i\sigma_i^y$ are spin raising and lowering operators. The parameter γ quantifies the nonreciprocity in the magnetization hopping. In the Hermitian limit $\gamma = 0$, the model reduces to the XXZ chain in the presence of both longitudinal and transverse fields, a standard example of a nonintegrable many-body system in the thermal phase [79]. The nonreciprocal XX coupling considered here is also closely connected to the asymmetric simple exclusion process [80–82]. In the limit $J = g = h = 0$, the model reduces essentially to the Hatano-Nelson model (6), for which the single-particle skin modes, as discussed above, have a trivial multifractal structure with vanishing multifractal dimensions. As we show below, this stands in marked contrast to the many-body skin effect, which exhibits multifractal behavior.

4.2 Multifractal scaling

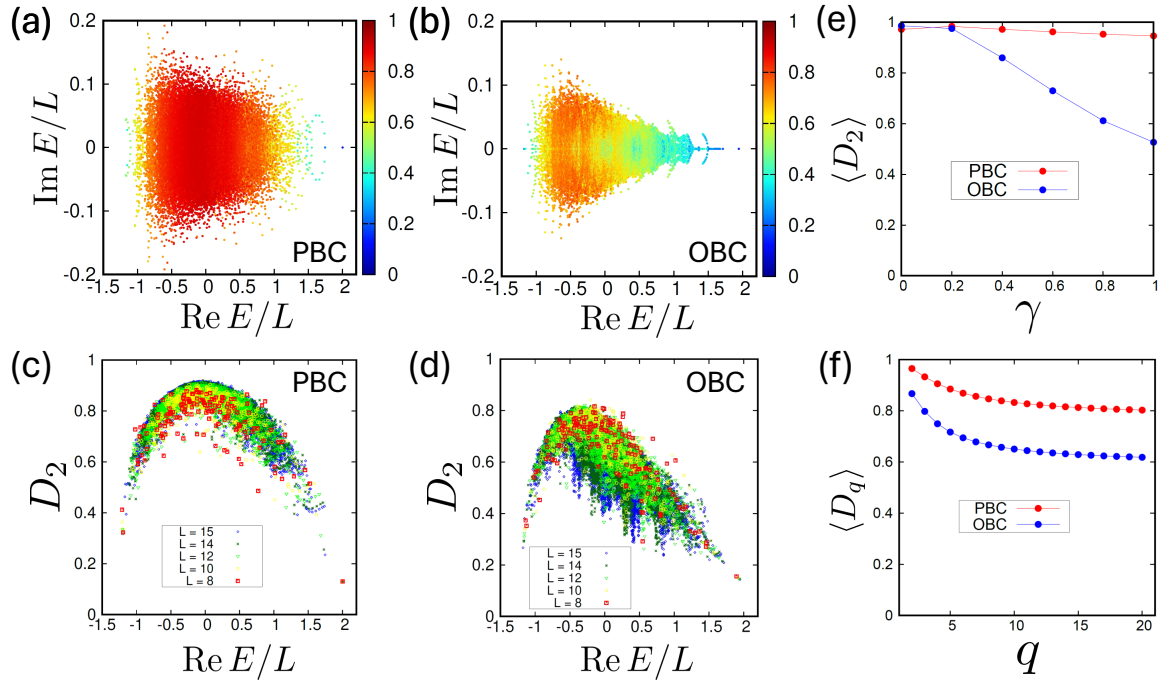


Figure 1: Multifractal scaling of the non-Hermitian spin chain in Eq. (13) ($t = 1/\sqrt{2}$, $J = 1$, $g = (5 + \sqrt{5})/8$, $h = (1 + \sqrt{5})/4$). (a, b) Eigenvalues ($\text{Re } E/L, \text{Im } E/L$) scaled by the system length $L = 15$ under the (a) periodic boundary conditions (PBC) and (b) open boundary conditions (OBC) ($\gamma = 0.8$). The color bars show the multifractal dimension D_2 for each right eigenstate. (c, d) Multifractal dimensions D_2 of individual right eigenstates as a function of $\text{Re } E/L$ for the different system lengths L under (c) PBC and (d) OBC ($\gamma = 0.8$). (e) Multifractal dimension $\langle D_2 \rangle$ averaged over all right eigenstates as functions of non-Hermiticity γ under both PBC (red dots) and OBC (blue dots). (f) q -dependence of average multifractal dimension $\langle D_q \rangle$ under both PBC (red dots) and OBC (blue dots) ($\gamma = 0.4$). Figure 1 adapted with permission from Ref. [67]. Copyright (2025) by the American Physical Society.

We now examine the multifractal scaling of the non-Hermitian spin chain in Eq. (13). Throughout this section, we use the spin configuration basis as the computational basis. The parameters are chosen to ensure nonintegrability in the Hermitian limit [79]. By exact diagonalization, we obtain the complex eigenvalues and the corresponding right eigenstates under both periodic and open boundary conditions.

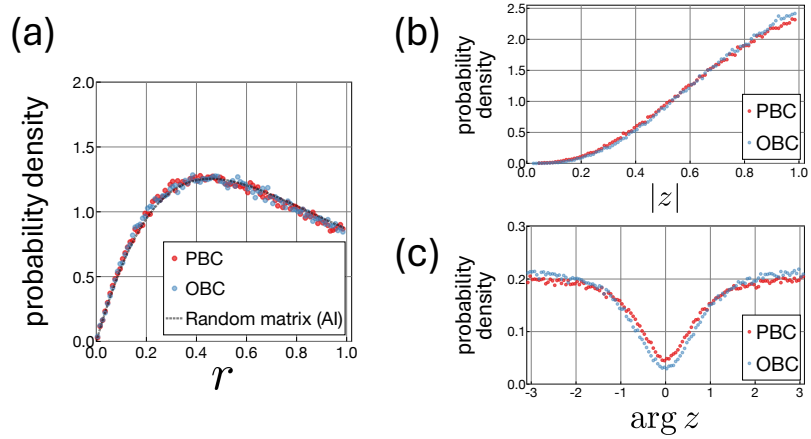


Figure 2: Level-spacing-ratio statistics of the non-Hermitian spin chain in Eq. (13) under PBC (red dots) and OBC (blue dots) ($t = 1/\sqrt{2}$, $\gamma = 0.6$, $J = 1$, $g = (5 + \sqrt{5})/8$, $h = (1 + \sqrt{5})/4$, $L = 14$). All data are taken away from the spectral edges and the symmetry line, and are averaged over 50 disorder realizations. (a) Spacing-ratio distribution r of singular values. The averages are $\langle r \rangle = 0.5297$ for PBC and $\langle r \rangle = 0.5299$ for OBC. The black dashed curve shows the analytical result for small non-Hermitian random matrices in class AI, namely $p(r) = 27(r+r^2)/[4(1+r+r^2)^{5/2}]$, with $\langle r \rangle = 4 - 2\sqrt{3} \simeq 0.5359$ [84]. (b, c) Level-spacing-ratio statistics of complex eigenvalues, shown for (b) the absolute value $|z|$ and (c) the argument $\arg z$. The averages are $\langle |z| \rangle = 0.7275$ and $\langle \cos \arg z \rangle = -0.1842$ for PBC, and $\langle |z| \rangle = 0.7365$ and $\langle \cos \arg z \rangle = -0.2355$ for OBC. For comparison, $10^4 \times 10^4$ non-Hermitian random matrices yield $\langle |z| \rangle = 0.7381$ and $\langle \cos \arg z \rangle = -0.2405$ [85]. Figure 2 adapted with permission from Ref. [67]. Copyright (2025) by the American Physical Society.

Figure 1 (a, b) shows the complex spectrum together with the multifractal dimension D_2 for individual right eigenstates. The spectrum changes significantly between periodic and open boundary conditions, signaling the skin effect. Note that the symmetry of the spectrum about the real axis originates from the time-reversal symmetry of the Hamiltonian, $H^* = H$. Under periodic boundary conditions, most eigenstates have $D_2 \simeq 1$, whereas under open boundary conditions, their counterparts exhibit substantially smaller multifractal dimensions. To further resolve the energy dependence, Fig. 1 (c, d) plots D_2 as a function of the real part of the energy for different system lengths. Under periodic boundary conditions, the distribution of multifractal dimensions forms a characteristic arc-like structure, reminiscent of that found in nonintegrable Hermitian many-body systems [83]. In particular, eigenstates in the middle of the spectrum tend toward $D_2 \simeq 1$ with increasing system length, while those near the spectral edges remain smaller. This deviation from unity near the spectral edges is naturally attributed to locality constraints of the Hamiltonian, in contrast to fully random matrices, where the corresponding distribution is flat [83]. By contrast, under open boundary conditions, multifractal dimensions remain at intermediate values even in the spectral bulk, indicating that the skin effect suppresses the effective occupation of the many-body Hilbert space.

To extract the multifractal dimension in the thermodynamic limits, we analyze the finite-size scaling of the participation entropy $S_q := \ln I_q / (1 - q)$, which is fitted as $\langle S_q \rangle = \langle D_q \rangle \ln \mathcal{N} + \langle c_q \rangle$ by averaging over all right eigenstates. Figure 1 (e) shows the resulting average multifractal dimension $\langle D_2 \rangle$ as a function of the nonreciprocity γ . While $\langle D_2 \rangle$ remains close to unity under periodic boundary conditions, it decreases with increasing γ under open boundary conditions, indicating that the skin effect enforces a progressively smaller occupation of the many-body Hilbert space. We also find a clear q dependence of the multifractal dimension [Fig. 1 (f)]. Taken together, these results show that the many-body skin effect exhibits multifractality in many-body Hilbert space, as opposed to the vanishing multifractal dimension of the single-particle skin effect. More detailed analyses of the parameter dependence, together with the corresponding results for integrable systems, can be found in Ref. [67].

4.3 Spectral statistics

In the previous subsection, we saw that the many-body skin effect gives rise to multifractal structure in many-body Hilbert space. In conventional multifractal quantum phases, such as many-body localized phases, multifractality is typically accompanied by Poisson spectral statistics, reflecting the absence of level repulsion due to local integrals of motion [86,87]. By contrast, the

multifractality of the many-body skin effect can coexist with random-matrix spectral statistics. This coexistence suggests a novel dissipative quantum-chaotic regime distinct from more conventional multifractal phases. To probe its quantum-chaotic nature, we examine both the singular-value statistics and the complex level-spacing statistics of the non-Hermitian Hamiltonian in Eq. (13). We note that spectral diagnostics of chaos have recently been extensively employed in open quantum systems [85, 88–99].

We first consider the spacing-ratio statistics of singular values. For an ordered set of singular values $\{s_n\}$ ($n = 1, 2, \dots, \mathcal{N}$), we define the ratio [84]

$$r_n := \min \left(\frac{s_{n+1} - s_n}{s_n - s_{n-1}}, \frac{s_n - s_{n-1}}{s_{n+1} - s_n} \right), \quad 0 \leq r_n \leq 1. \quad (14)$$

To remove unwanted symmetries, we add a weak disordered term $\sum_{i=1}^L \varepsilon_i \sigma_i^z \sigma_{i+1}^z$, where each ε_i is uniformly distributed in $[-0.1, 0.1]$. As shown in Fig. 2 (a), the singular-value statistics under both periodic and open boundary conditions are in close agreement with the random-matrix prediction. In particular, the averaged spacing ratio takes $\langle r \rangle = 0.5297$ for periodic boundary conditions and $\langle r \rangle = 0.5299$ for open boundary conditions, both close to the random-matrix value $\langle r \rangle = 0.5359$.

We next analyze the statistics of complex level-spacing ratios [85],

$$z_n := \frac{E_n^{\text{NN}} - E_n}{E_n^{\text{NNN}} - E_n}, \quad (15)$$

where E_n^{NN} (E_n^{NNN}) is the nearest (next-nearest) eigenvalue to E_n in the complex-energy plane. The numerical distributions of both $|z|$ and $\arg z$ are likewise consistent with non-Hermitian random-matrix statistics, as shown in Fig. 2 (b, c). The small deviation observed under periodic boundary conditions is naturally attributed to the residual effect of average translation symmetry. Specifically, we obtain $\langle |z| \rangle = 0.7275$ and $\langle \cos \arg z \rangle = -0.1842$ for periodic boundary conditions, and $\langle |z| \rangle = 0.7365$ and $\langle \cos \arg z \rangle = -0.2355$ for open boundary conditions, in good agreement with the corresponding random-matrix values $\langle |z| \rangle = 0.7381$ and $\langle \cos \arg z \rangle = -0.2405$.

Taken together, these results highlight a characteristic feature of the many-body skin effect: the coexistence of multifractal eigenstates and random-matrix spectral statistics, unlike many-body localized phases (Table 1).

5 Tree geometry and analytic multifractality

In this section, we turn to a non-Hermitian model on the Cayley tree [100]. We begin by explaining the motivation for introducing the tree model in the present context, and then define the model. We subsequently construct the relevant basis states and derive the exact eigenstates. Finally, we compute the multifractal dimensions and discuss the degeneracy of eigenstates.

5.1 Motivation

The previous section numerically uncovered the multifractal structure of the many-body skin effect. While this analysis demonstrates the emergence of multifractality, the relation between the resulting occupation profile and the underlying Hilbert-space structure is not yet fully transparent. To gain analytical insight, it is therefore useful to consider a simpler setting in which these structural effects can be examined more transparently.

A key starting point is to view many-body Hilbert space as a graph. In this picture, each spin configuration basis state corresponds to a node, and the Hamiltonian connects nearby nodes through its off-diagonal matrix elements. Because the number of connected basis states grows hierarchically, the resulting graph is often locally tree-like in character. Such graph-based descriptions were originally discussed in the context of interacting quantum dots [101], and have since been employed more broadly in studies of multifractality in many-body systems [102].

Motivated by this spirit, we now turn to a non-Hermitian model on a Cayley tree as an analytically tractable toy model for the many-body Hilbert space. Although the Cayley tree does not capture the full complexity of the many-body problem, it retains an essential feature of many-body Hilbert space, namely its hierarchical branching structure. As shown below, the competition between the hierarchical growth of Hilbert space and nonreciprocity determines the multifractal dimensions exactly and clarifies how the occupation profile of skin modes is shaped by the underlying Hilbert-space structure.

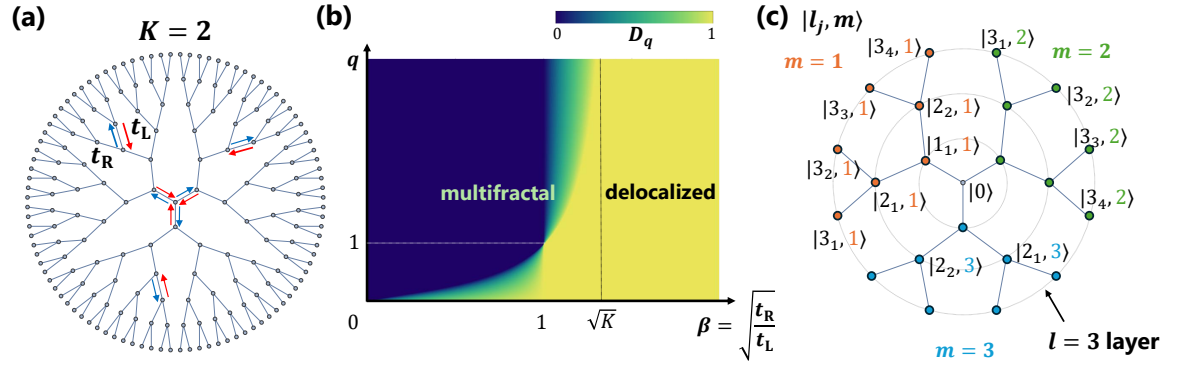


Figure 3: (a) Sketch of the model with nonreciprocal hopping on the Cayley tree for branching number $K = 2$. The number of layers is $M = 6$. The hopping amplitude from the boundary to the center (from the center to the boundary) is t_L (t_R). (b) Phase diagram of the multifractal dimension D_q . For $K \geq 2$, the symmetric eigenstates are localized in the limit $\beta \rightarrow 0$, delocalized for $\beta > \sqrt{K}$, and multifractal in the intermediate regime $0 < \beta < \sqrt{K}$. (c) Sketch of the symmetric basis construction in the case $K = 2$. The symmetric basis states are constructed by linear superposition of the position basis $|l, j, m\rangle$. Figure 3 adapted with permission from Ref. [100]. Copyright (2025) by the American Physical Society.

5.2 Model

We study a non-Hermitian model defined on a Cayley tree. A Cayley tree is a rooted graph characterized by a fixed branching number K : apart from the outermost sites, each node connects to one node in the preceding layer and to K nodes in the following layer, so that each bulk node has $K + 1$ neighbors [Fig. 3 (a)]. The graph is built recursively from a central root node. Starting from this root, one first attaches $K + 1$ nodes to form the first layer. Each node in a given layer then generates K descendants in the next layer. After repeating this construction up to depth M , one obtains an M -layer Cayley tree with branching number K . By construction, all nodes within the same layer are at equal graph distance from the root. Figure 3 (a) shows the case with $M = 6$ and $K = 2$.

To realize the non-Hermitian skin effect on the Cayley tree, we consider the following nonreciprocal Hamiltonian:

$$H = t_R \sum_{\langle i > j \rangle} |i\rangle \langle j| + t_L \sum_{\langle i < j \rangle} |i\rangle \langle j|, \quad (16)$$

where $t_R, t_L > 0$ denote the hopping amplitudes. Here, $\sum_{\langle i > j \rangle}$ ($\sum_{\langle i < j \rangle}$) denotes the sum over neighboring nodes i and j such that node j lies closer to (farther from) the central node than node i [see Fig. 3 (a)]. Nonreciprocity is introduced when $\beta \neq 1$ ($\beta := \sqrt{t_R/t_L}$), or equivalently when $t_R \neq t_L$. For $t_R < t_L$ ($t_R > t_L$), the asymmetric hopping biases the particle motion toward the central node (the surface nodes). A non-Hermitian tree model was also studied independently [103], while another independent study considered a different context [104].

5.3 Symmetric sector

The full Hilbert-space dimension for an M -layer Cayley tree with branching number K in Eq. (16) is

$$\mathcal{N} = 1 + (K + 1) \sum_{l=1}^M K^{l-1} = 1 + (K + 1) \frac{K^M - 1}{K - 1}. \quad (17)$$

While the Hamiltonian in Eq. (16) is exactly solved [100], much of the following discussion is devoted to its symmetric sector for simplicity.

The symmetric sector is spanned by basis states constructed by uniformly superposing nodes within each layer of a given branch, as explained in detail below. We choose the central node as one of the symmetric basis states as $|0\rangle := |0\rangle$. Here, $|\dots\rangle$ denotes the original position basis, whereas $|\dots\rangle$ denotes symmetric basis states. Other symmetric states on the l th layer of branch m are constructed as [Fig. 3 (c)]

$$|l\rangle_m := \frac{1}{\sqrt{K^{l-1}}} \sum_{j=1}^{K^{l-1}} |l, j, m\rangle, \quad l = 1, \dots, M, \quad m = 1, \dots, K + 1. \quad (18)$$

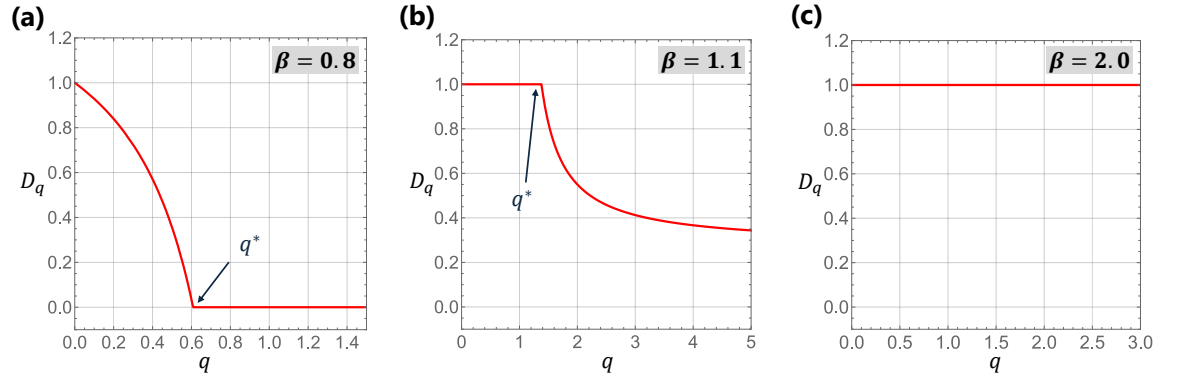


Figure 4: Dependence of the multifractal dimensions D_q on q in the three regimes: (a) $0 < \beta < 1$, (b) $1 < \beta < \sqrt{K}$, and (c) $\beta > \sqrt{K}$. The curves are shown for $K = 2$, with representative values $\beta = 0.8, 1.1$, and 2.0 for panels (a), (b), and (c), respectively. Figure 4 adapted with permission from Ref. [100]. Copyright (2025) by the American Physical Society.

An eigenstate in this symmetric sector is expanded as $|\Psi\rangle = \psi_0|0\rangle + \sum_{l=1}^M \sum_{m=1}^{K+1} \psi_{l,m}|l\rangle_m$. We refer to the eigenstate in this symmetric sector as symmetric eigenstates. Details of the complementary nonsymmetric basis construction are given in Ref. [100].

Within the symmetric sector, the eigenvalue equation reduces to a set of recurrence relations. In particular, for the class of solutions with $\psi_0 = 0$, one finds ¹

$$E\psi_{l,m} = \sqrt{K} t_R \psi_{l-1,m} + \sqrt{K} t_L \psi_{l+1,m}, \quad (19)$$

$$\psi_{0,m} = \psi_{M+1,m} = 0, \quad (20)$$

$$0 = \sum_{m=1}^{K+1} \psi_{1,m}, \quad (21)$$

for $l = 1, \dots, M$ and $m = 1, \dots, K + 1$. The first two lines are identical to the eigenvalue problem of the Hatano–Nelson chain, and thus yield

$$\psi_{l,m}^{(n)} = \beta^l \sin(\theta_n l), \quad E_n = 2\sqrt{K t_R t_L} \cos \theta_n, \quad (22)$$

with $\beta = \sqrt{t_R/t_L}$ and $\theta_n = n\pi/(M + 1)$ for $n = 1, \dots, M$. Accordingly, the symmetric eigenstates take the form

$$|\Psi_n\rangle = \sum_{m=1}^{K+1} \sum_{l=1}^M c_m \psi_{l,m}^{(n)} |l\rangle_m, \quad (23)$$

where the coefficients satisfy $\sum_{m=1}^{K+1} c_m = 0$. This constraint reduces the branch degeneracy from $K + 1$ to K , so that the symmetric sector contains KM linearly independent eigenstates. It should be noted that the obtained symmetric eigenstates are not degenerate with any of the remaining eigenstates if $M + 1$ is chosen to be a prime number [100]. Since the symmetric solutions are free from M -dependent degeneracy at each n , the multifractal dimensions are uniquely determined in this sector, making it particularly tractable.

5.4 Exact multifractal dimension

We now evaluate the multifractal dimensions analytically. Substituting the exact symmetric eigenstates in Eq. (23) into the definition of the inverse participation ratio in the position basis $|l, j, m\rangle$, we obtain

$$I_q = \left[\frac{\beta^2 - 1}{\beta^2(\beta^{2M} - 1)} \right]^q \frac{1 - \left(\frac{\beta^{2q}}{K^{q-1}} \right)^M}{\beta^{-2q} - K^{1-q}} \sum_{m=1}^{K+1} |c_m|^{2q}. \quad (24)$$

Importantly, while the Hilbert-space dimension grows as $\mathcal{N} \propto K^M$ because of the hierarchical branching of the tree, the inverse participation ratio scales either as $I_q \propto \beta^{-2qM}$ or

¹Here we introduce $\psi_{0,m} := \psi_0/\sqrt{K}$ for notational convenience.

$I_q \propto (\beta^{2q}/K^{q-1})^M$ due to the skin effect. The competition between geometric branching K and nonreciprocal hopping β gives the multifractal properties of the skin modes. Depending on β , the multifractal dimensions are classified into three distinct regimes, for which closed-form expressions can be derived analytically.

For $0 < \beta < 1$, the multifractal dimensions are given by

$$D_q = \begin{cases} 1 - \frac{q}{q-1} \frac{\log(\beta^2)}{\log K}, & (q < q^*), \\ 0, & (q > q^*), \end{cases} \quad (25)$$

where

$$q^* := \frac{\log K}{\log K - \log(\beta^2)}. \quad (26)$$

Since D_q depends explicitly on q , this regime exhibits multifractality [Fig. 4 (a)]. This contrasts with the vanishing multifractal dimensions of single-particle skin modes in one dimension discussed in Sec. 3, and reflects the unique scaling behavior of skin modes on a hierarchical lattice. As $\beta \rightarrow 0$, the crossover value q^* tends to zero, and correspondingly D_q vanishes for all q . This limit describes complete localization of the eigenstates around the central node, induced by strong inward nonreciprocity ($t_L \gg t_R$).

For $1 < \beta < \sqrt{K}$, the multifractal dimensions are given by

$$D_q = \begin{cases} 1, & (q < q^*), \\ \frac{q}{q-1} \frac{\log(\beta^2)}{\log K}, & (q > q^*). \end{cases} \quad (27)$$

As in the previous regime, the explicit q dependence of D_q signals multifractality [Fig. 4 (b)]. A particularly notable feature appears as $\beta \rightarrow \sqrt{K}$, where the crossover value q^* diverges and the multifractal dimensions approach $D_q = 1$ for all q . This corresponds to complete delocalization of the eigenstates over the Cayley tree. Unlike the localized limit $D_q = 0$, which is reached only as $\beta \rightarrow 0$, full delocalization already occurs at the finite threshold $\beta = \sqrt{K}$. Physically, even when hopping is biased outward, the wave-function amplitude is redistributed over K descendant branches at each node of the tree. As a result, outward hopping must be strong enough to compensate for this repeated branching. The condition $\beta = \sqrt{K}$ is precisely the point at which these two effects balance, leading to fully delocalized skin modes. We also note that a finite value of $D_{q \rightarrow \infty} = \log(\beta^2)/\log K$ means that even the largest wave-function amplitudes are not concentrated on a finite number of sites, but instead scale over a Hilbert-space subset of nonzero effective dimension.

For $\beta > \sqrt{K}$, the multifractal dimensions are

$$D_q = 1, \quad (28)$$

so that the eigenstates are fully delocalized in Hilbert space [Fig. 4 (c)]. In the extreme limit $\beta \rightarrow \infty$, the wave function is pushed toward the outer boundary of the tree. However, since the number of boundary nodes increases exponentially with the number of layers and dominates the Hilbert-space volume in the thermodynamic limit, this boundary accumulation is still delocalized from the viewpoint of Hilbert-space occupation. Accordingly, the states remain characterized by $D_q = 1$.

For both $0 < \beta < 1$ and $1 < \beta < \sqrt{K}$, the symmetric eigenstates exhibit multifractal statistics. The nature of this multifractality, however, differs qualitatively between the two regimes [Fig. 4 (a, b)]. To make this distinction more explicit, we further examine the exponents τ_q and the corresponding multifractal spectrum f_α . For $0 < \beta < 1$, we obtain

$$\tau_q = \begin{cases} \frac{1}{q^*}(q - q^*), & (q < q^*), \\ 0, & (q > q^*), \end{cases} \quad f_\alpha = \begin{cases} q^* \alpha, & \left(0 < \alpha < \frac{1}{q^*}\right), \\ -\infty, & (\text{otherwise}), \end{cases} \quad (29)$$

whereas for $1 < \beta < \sqrt{K}$,

$$\tau_q = \begin{cases} q - 1, & (q < q^*), \\ \frac{\log(\beta^2)}{\log K} q, & (q > q^*), \end{cases} \quad f_\alpha = \begin{cases} q^* \alpha + (1 - q^*), & \left(1 - \frac{1}{q^*} < \alpha < 1\right), \\ -\infty, & (\text{otherwise}). \end{cases} \quad (30)$$

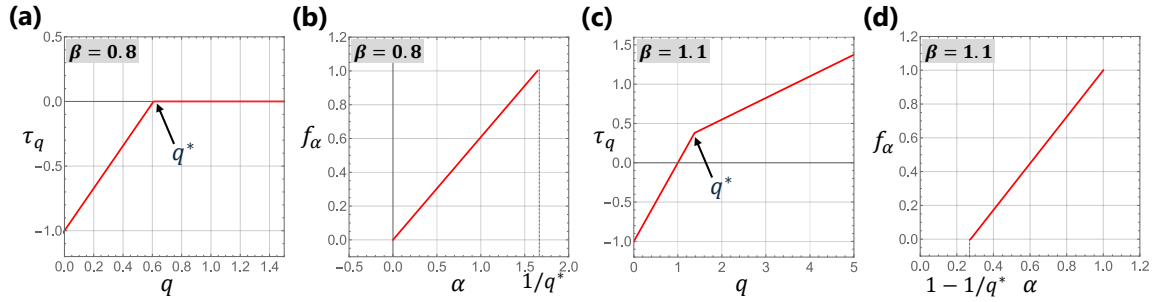


Figure 5: The dependence on q of the exponent τ_q , and the dependence on α of the multifractal spectrum f_α , displayed for $\beta = 0.8$ (a1, a2) and for $\beta = 1.1$ (b1, b2). The data are plotted for the case $K = 2$. Figure 5 adapted with permission from Ref. [100]. Copyright (2025) by the American Physical Society.

For $0 < \beta < 1$, the exponent τ_q vanishes for $q > q^*$ [Fig. 5 (a)]. This behavior is reminiscent of sparse multifractal states, where the moments at large q are dominated by a small number of exceptionally large amplitudes. Indeed, in the Anderson transition in high dimensions, one finds $\tau_q = 0$ above a finite threshold in the $d \rightarrow \infty$ limit [105–109]. Equation (29) shows that the skin modes on the Cayley tree exhibit an analogous structure, although the threshold now depends on the parameter q^* . Physically, the moment I_q for large q is controlled by the largest wave-function components, and the condition $\tau_q = 0$ therefore implies that the state is strongly concentrated near the central region of the tree, consistent with Eq. (22). By contrast, for smaller q , which probe the more broadly distributed part of the wave function, the states retain multifractal character. The corresponding multifractal spectrum f_α is peaked near $\alpha \simeq 1/q^*$ [Fig. 5 (b)], indicating that the wave function scales locally as $|\psi_j|^2 \propto \mathcal{N}^{-1/q^*}$ over a broad set of sites. We also note that the nonanalyticity of τ_q at $q = q^*$, together with the saturation $\tau_q = 0$ for $q > q^*$, signals a *freezing transition* in the multifractal statistics. Such frozen behavior has previously been discussed for the Anderson transition on the Bethe lattice [110], the two-dimensional random Dirac model [111], and the Rosenzweig-Porter random matrix model [10]. Here, however, the same type of singular multifractal structure arises from nonreciprocity rather than disorder.

For $1 < \beta < \sqrt{K}$, by contrast, the exponent τ_q remains positive for all $q > 1$ [Fig. 5 (c)]. This is different both from the $0 < \beta < 1$ regime and from sparse multifractality at high-dimensional Anderson transitions, where τ_q saturates to zero at large q . The absence of such saturation implies that the wave function does not develop a small set of sharply dominant peaks, even though it remains multifractal. This is also reflected in the multifractal spectrum f_α , which is peaked near $\alpha \simeq 1$ [Fig. 5 (d)]. Accordingly, the wave-function amplitudes scale as $|\psi_j|^2 \propto \mathcal{N}^{-1}$ over most of the occupied sites, consistent with the fact that $D_q = 1$ for small q in Fig. 4 (b).

5.5 Multifractal dimensions of degenerate states

So far, we have focused on the symmetric eigenstates, for which the multifractal dimensions are uniquely defined. By contrast, the remaining non-symmetric eigenstates on the Cayley tree are extensively degenerate, and their multifractal dimensions are therefore not uniquely determined. In this subsection, we show explicitly that the multifractal dimension depends on the choice of linear combination within the degenerate subspace, and we also examine the effect of weak disorder.

For $K = 2$, this dependence can be seen by comparing two different constructions of degenerate eigenstates. When one chooses symmetry-adapted linear combinations that are simultaneous eigenstates of the branch-permutation symmetries of the Cayley tree, the resulting states are more uniformly distributed over the branches and exhibit relatively large values of D_2 [Fig. 6 (a)]. By contrast, generic linear combinations chosen at random lead to a broader distribution and smaller values of D_2 , explicitly demonstrating that the multifractal dimension of the degenerate states depends on the particular linear combination chosen [Fig. 6 (b)].

We next consider weak disorder, which is expected in realistic experimental settings. Specifically, we consider

$$H_{\text{dis}} = H + \sum_{j=1}^{\mathcal{N}} U_j |j\rangle \langle j|, \quad (31)$$

where $U_j \in [-u, u]$ is a random on-site potential. In this case, disorder favors linear combinations that are more localized on particular branches, leading to smaller values of D_2 for the

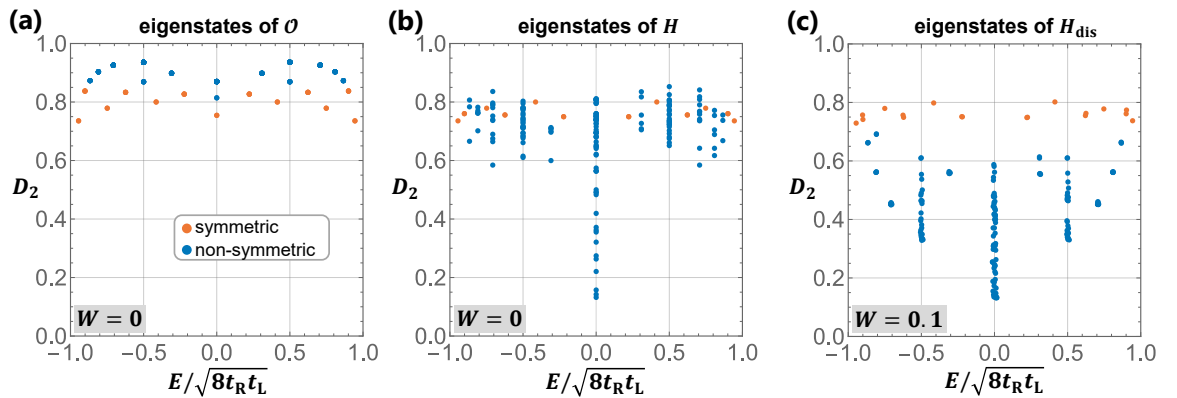


Figure 6: The multifractal dimension D_2 as a function of the rescaled energy $E/\sqrt{8t_R t_L}$ for a Cayley tree with $K = 2$, ($M + 1 = 7$, $t_R = 1.1$, $t_L = 0.9$). (a, b) In the absence of disorder ($W = 0$) and (c) in the presence of weak disorder ($W = 0.1$). Data for symmetric (non-symmetric) eigenstates are shown in orange (blue). In panel (a), we consider simultaneous eigenstates of the commuting set $\mathcal{O} = \{H, C_3, C_{2,1}, \dots, C_{2,M-1}\}$, where C_3 denotes the threefold rotation that cyclically permutes the three main branches attached to the central node, and $C_{2,l}$ denotes the twofold swap symmetry at layer l , which exchanges the two descendant subbranches branching from each node in that layer. In panel (b), we show generic eigenstates of the Hamiltonian H without imposing such symmetry-adapted linear combinations. Figure 6 adapted with permission from Ref. [100]. Copyright (2025) by the American Physical Society.

non-symmetric sector. The symmetric eigenstates, on the other hand, are not subject to such extensive degeneracy and remain essentially unaffected by weak disorder. Thus, while the multifractal dimensions of symmetric eigenstates are robust, the highly degenerate non-symmetric eigenstates are strongly sensitive both to the choice of linear combinations and to weak disorder.

6 Conclusion and outlook

In this article, we have reviewed the multifractal aspects of the non-Hermitian skin effect across a wide range of settings, from single-particle systems to many-body and tree models. A central message is that the many-body skin effect gives rise to multifractal structures in many-body Hilbert space, whereas conventional single-particle skin modes on crystalline lattices do not exhibit multifractality. We have also highlighted that this multifractality can coexist with random-matrix spectral statistics, unlike conventional multifractal phases such as many-body localized phases. Furthermore, the non-Hermitian model on the Cayley tree provides an analytically tractable setting in which the competition between hierarchical branching and nonreciprocity determines the multifractal dimensions exactly. Taken together, these results provide a unified perspective on multifractal structures associated with the non-Hermitian skin effect.

In the context of Anderson localization and many-body localization, (multi)fractality has been effectively described by random-matrix models such as power-law banded random matrices [112] and the Rosenzweig-Porter model [10, 113], where multifractal dimensions can be obtained analytically. While several works have explored non-Hermitian extensions of such settings, including the absence of a fractal phase in the non-Hermitian Rosenzweig-Porter model [114], much remains to be understood about multifractality in non-Hermitian random-matrix models.

Finally, very recently, nonlinear extensions of the non-Hermitian skin effect have begun to attract increasing attention [115–120]. The results reviewed here suggest that skin modes are not always most naturally characterized in real space alone, but may instead admit a quantitative description in an appropriate space, such as Hilbert space or graph space, depending on the setting. From this viewpoint, it would be natural to ask whether nonlinear skin effects may also admit a useful characterization in function space [120]. Exploring this possibility remains an important direction for future research.

Acknowledgments

I am deeply grateful to Kohei Kawabata for introducing me to this topic and for teaching me most of the findings in Ref. [67]. I also thank Askar A. Iliasov, Titus Neupert, Tomáš Bzdušek, and Tsuneya Yoshida for related collaborations and valuable suggestions. I further thank Tsuneya Yoshida for his continued encouragement. I also thank Jacopo Gliozzi, Taylor L. Hughes, David A.

Huse, and Shinsei Ryu for valuable feedback on these works. Finally, I would like to thank the editors for inviting me to write this paper.

Funding

This work was supported by JSPS Research Fellow No. 24KJ1445.

References

- [1] Thomas C. Halsey, Mogens H. Jensen, Leo P. Kadanoff, Itamar Procaccia, and Boris I. Shraiman. Fractal measures and their singularities: The characterization of strange sets. *Phys. Rev. A*, 33:1141–1151, Feb 1986.
- [2] Ferdinand Evers and Alexander D. Mirlin. Anderson transitions. *Rev. Mod. Phys.*, 80:1355–1417, Oct 2008.
- [3] F. Wegner. Inverse participation ratio in $2 + \varepsilon$ dimensions. *Z Physik B*, 36:209, 1980.
- [4] C. Castellani and L. Peliti. Multifractal wavefunction at the localisation threshold. *J. Phys. A*, 19:L429, 1986.
- [5] Michael Schreiber and Heiko Grussbach. Multifractal wave functions at the Anderson transition. *Phys. Rev. Lett.*, 67:607–610, Jul 1991.
- [6] Christopher Mudry, Claudio Chamon, and Xiao-Gang Wen. Two-dimensional conformal field theory for disordered systems at criticality. *Nucl. Phys. B*, 466:383, 1996.
- [7] F. Evers and A. D. Mirlin. Fluctuations of the Inverse Participation Ratio at the Anderson Transition. *Phys. Rev. Lett.*, 84:3690–3693, Apr 2000.
- [8] A. D. Mirlin and F. Evers. Multifractality and critical fluctuations at the Anderson transition. *Phys. Rev. B*, 62:7920–7933, Sep 2000.
- [9] David J. Luitz, Nicolas Laflorencie, and Fabien Alet. Many-body localization edge in the random-field Heisenberg chain. *Phys. Rev. B*, 91:081103, Feb 2015.
- [10] V E Kravtsov, I M Khaymovich, E Cuevas, and M Amini. A random matrix model with localization and ergodic transitions. *New Journal of Physics*, 17(12):122002, dec 2015.
- [11] Maksym Serbyn, Z. Papić, and Dmitry A. Abanin. Thouless energy and multifractality across the many-body localization transition. *Phys. Rev. B*, 96:104201, Sep 2017.
- [12] Nicolas Macé, Fabien Alet, and Nicolas Laflorencie. Multifractal Scalings Across the Many-Body Localization Transition. *Phys. Rev. Lett.*, 123:180601, Oct 2019.
- [13] A. Zabalo, M. J. Gullans, J. H. Wilson, R. Vasseur, A. W. W. Ludwig, S. Gopalakrishnan, David A. Huse, and J. H. Pixley. Operator Scaling Dimensions and Multifractality at Measurement-Induced Transitions. *Phys. Rev. Lett.*, 128:050602, Feb 2022.
- [14] Jason Iaconis and Xiao Chen. Multifractality in nonunitary random dynamics. *Phys. Rev. B*, 104:214307, Dec 2021.
- [15] Piotr Sierant and Xhek Turkeshi. Universal Behavior beyond Multifractality of Wave Functions at Measurement-Induced Phase Transitions. *Phys. Rev. Lett.*, 128:130605, Apr 2022.
- [16] Shunyu Yao and Zhong Wang. Edge States and Topological Invariants of Non-Hermitian Systems. *Phys. Rev. Lett.*, 121:086803, Aug 2018.
- [17] M. S. Rudner and L. S. Levitov. Topological Transition in a Non-Hermitian Quantum Walk. *Phys. Rev. Lett.*, 102:065703, 2009.
- [18] M. Sato, K. Hasebe, K. Esaki, and M. Kohmoto. Time-Reversal Symmetry in Non-Hermitian Systems. *Prog. Theor. Phys.*, 127:937, 2012.
- [19] K. Esaki, M. Sato, K. Hasebe, and M. Kohmoto. Edge states and topological phases in non-Hermitian systems. *Phys. Rev. B*, 84:205128, 2011.

- [20] Y. C. Hu and T. L. Hughes. Absence of topological insulator phases in non-Hermitian PT -symmetric Hamiltonians. *Phys. Rev. B*, 84:153101, 2011.
- [21] H. Schomerus. Topologically protected midgap states in complex photonic lattices. *Opt. Lett.*, 38:1912, 2013.
- [22] D. Leykam, K. Y. Bliokh, C. Huang, Y. D. Chong, and F. Nori. Edge Modes, Degeneracies, and Topological Numbers in Non-Hermitian Systems. *Phys. Rev. Lett.*, 118:040401, 2017.
- [23] Y. Xu, S.-T. Wang, and L.-M. Duan. Weyl Exceptional Rings in a Three-Dimensional Dissipative Cold Atomic Gas. *Phys. Rev. Lett.*, 118:045701, 2017.
- [24] H. Shen, B. Zhen, and L. Fu. Topological Band Theory for Non-Hermitian Hamiltonians. *Phys. Rev. Lett.*, 120:146402, 2018.
- [25] Vladyslav Kozii and Liang Fu. Non-Hermitian topological theory of finite-lifetime quasiparticles: Prediction of bulk Fermi arc due to exceptional point. *Phys. Rev. B*, 109:235139, Jun 2024.
- [26] Zongping Gong, Yuto Ashida, Kohei Kawabata, Kazuaki Takasan, Sho Higashikawa, and Masahito Ueda. Topological Phases of Non-Hermitian Systems. *Phys. Rev. X*, 8:031079, Sep 2018.
- [27] Kohei Kawabata, Ken Shiozaki, Masahito Ueda, and Masatoshi Sato. Symmetry and Topology in Non-Hermitian Physics. *Phys. Rev. X*, 9:041015, Oct 2019.
- [28] Xin-Ran Ma, Kui Cao, Xiao-Ran Wang, Zheng Wei, Qian Du, and Su-Peng Kou. Non-hermitian chiral skin effect. *Phys. Rev. Res.*, 6:013213, Feb 2024.
- [29] Frank Schindler, Kaiyuan Gu, Biao Lian, and Kohei Kawabata. Hermitian Bulk – Non-Hermitian Boundary Correspondence. *PRX Quantum*, 4:030315, Aug 2023.
- [30] Daichi Nakamura, Kazuya Inaka, Nobuyuki Okuma, and Masatoshi Sato. Universal Platform of Point-Gap Topological Phases from Topological Materials. *Phys. Rev. Lett.*, 131:256602, Dec 2023.
- [31] Federico Roccati, Miguel Bello, Zongping Gong, Masahito Ueda, Francesco Ciccarello, Aurélie Chenu, and Angelo Carollo. Hermitian and non-hermitian topology from photon-mediated interactions. *Nature Communications*, 15(1):2400, Mar 2024.
- [32] Shu Hamanaka, Tsuneya Yoshida, and Kohei Kawabata. Non-Hermitian Topology in Hermitian Topological Matter. *Phys. Rev. Lett.*, 133:266604, Dec 2024.
- [33] Yusuke O. Nakai, Reuel Dsouza, Daichi Nakamura, Shu Hamanaka, Andreas P. Schnyder, and Masatoshi Sato. Callan-Rubakov effects in topological insulators, 2025. arXiv:2502.16729.
- [34] Fei Song, Shunyu Yao, and Zhong Wang. Non-Hermitian Skin Effect and Chiral Damping in Open Quantum Systems. *Phys. Rev. Lett.*, 123:170401, Oct 2019.
- [35] Chun-Hui Liu, Kai Zhang, Zhesen Yang, and Shu Chen. Helical damping and dynamical critical skin effect in open quantum systems. *Phys. Rev. Res.*, 2:043167, Oct 2020.
- [36] Taiki Haga, Masaya Nakagawa, Ryusuke Hamazaki, and Masahito Ueda. Liouvillian Skin Effect: Slowing Down of Relaxation Processes without Gap Closing. *Phys. Rev. Lett.*, 127:070402, Aug 2021.
- [37] Takashi Mori and Tatsuhiko Shirai. Resolving a Discrepancy between Liouvillian Gap and Relaxation Time in Boundary-Dissipated Quantum Many-Body Systems. *Phys. Rev. Lett.*, 125:230604, Dec 2020.
- [38] Kohei Kawabata, Tokiro Numasawa, and Shinsei Ryu. Entanglement Phase Transition Induced by the Non-Hermitian Skin Effect. *Phys. Rev. X*, 13:021007, Apr 2023.
- [39] Samuel E. Begg and Ryo Hanai. Quantum Criticality in Open Quantum Spin Chains with Nonreciprocity. *Phys. Rev. Lett.*, 132:120401, Mar 2024.

- [40] Ruizhe Shen, Tianqi Chen, Bo Yang, and Ching Hua Lee. Observation of the non-hermitian skin effect and fermi skin on a digital quantum computer. *Nature Communications*, 16(1):1340, Feb 2025.
- [41] Tsuneya Yoshida, Song-Bo Zhang, Titus Neupert, and Norio Kawakami. Non-Hermitian Mott Skin Effect. *Phys. Rev. Lett.*, 133:076502, Aug 2024.
- [42] Jacopo Gliozzi, Giuseppe De Tomasi, and Taylor L. Hughes. Many-Body Non-Hermitian Skin Effect for Multipoles. *Phys. Rev. Lett.*, 133:136503, Sep 2024.
- [43] Martin Brandenbourger, Xander Locsin, Edan Lerner, and Corentin Coulais. Non-reciprocal robotic metamaterials. *Nature Communications*, 10(1):4608, Oct 2019.
- [44] Ananya Ghatak, Martin Brandenbourger, Jasper van Wezel, and Corentin Coulais. Observation of non-hermitian topology and its bulk–edge correspondence in an active mechanical metamaterial. *Proceedings of the National Academy of Sciences*, 117(47):29561–29568, 2020.
- [45] Xiujuan Zhang, Yuan Tian, Jian-Hua Jiang, Ming-Hui Lu, and Yan-Feng Chen. Observation of higher-order non-hermitian skin effect. *Nature Communications*, 12(1):5377, Sep 2021.
- [46] T. Helbig, T. Hofmann, S. Imhof, M. Abdelghany, T. Kiessling, L. W. Molenkamp, C. H. Lee, A. Szameit, M. Greiter, and R. Thomale. Generalized bulk–boundary correspondence in non-hermitian topoelectrical circuits. *Nature Physics*, 16(7):747–750, Jul 2020.
- [47] Tobias Hofmann, Tobias Helbig, Frank Schindler, Nora Salgo, Marta Brzezińska, Martin Greiter, Tobias Kiessling, David Wolf, Achim Vollhardt, Anton Kabaši, Ching Hua Lee, Ante Bilušić, Ronny Thomale, and Titus Neupert. Reciprocal skin effect and its realization in a topoelectrical circuit. *Phys. Rev. Res.*, 2:023265, Jun 2020.
- [48] Lei Xiao, Tianshu Deng, Kunkun Wang, Gaoyan Zhu, Zhong Wang, Wei Yi, and Peng Xue. Non-hermitian bulk–boundary correspondence in quantum dynamics. *Nature Physics*, 16(7):761–766, Jul 2020.
- [49] Qian Liang, Dizhou Xie, Zhaoli Dong, Haowei Li, Hang Li, Bryce Gadway, Wei Yi, and Bo Yan. Dynamic Signatures of Non-Hermitian Skin Effect and Topology in Ultracold Atoms. *Phys. Rev. Lett.*, 129:070401, Aug 2022.
- [50] Wei Gou, Tao Chen, Dizhou Xie, Teng Xiao, Tian-Shu Deng, Bryce Gadway, Wei Yi, and Bo Yan. Tunable Nonreciprocal Quantum Transport through a Dissipative Aharonov-Bohm Ring in Ultracold Atoms. *Phys. Rev. Lett.*, 124:070402, Feb 2020.
- [51] Kazuki Yokomizo and Shuichi Murakami. Non-Bloch Band Theory of Non-Hermitian Systems. *Phys. Rev. Lett.*, 123:066404, Aug 2019.
- [52] Hong-Yi Wang, Fei Song, and Zhong Wang. Amoeba Formulation of Non-Bloch Band Theory in Arbitrary Dimensions. *Phys. Rev. X*, 14:021011, Apr 2024.
- [53] Kai Zhang, Zhesen Yang, and Chen Fang. Correspondence between Winding Numbers and Skin Modes in Non-Hermitian Systems. *Phys. Rev. Lett.*, 125:126402, Sep 2020.
- [54] Nobuyuki Okuma, Kohei Kawabata, Ken Shiozaki, and Masatoshi Sato. Topological Origin of Non-Hermitian Skin Effects. *Phys. Rev. Lett.*, 124:086801, Feb 2020.
- [55] Sen Mu, Ching Hua Lee, Linhu Li, and Jiangbin Gong. Emergent Fermi surface in a many-body non-Hermitian fermionic chain. *Phys. Rev. B*, 102:081115, Aug 2020.
- [56] Eunwoo Lee, Hyunjik Lee, and Bohm-Jung Yang. Many-body approach to non-Hermitian physics in fermionic systems. *Phys. Rev. B*, 101:121109, Mar 2020.
- [57] Dan-Wei Zhang, Yu-Lian Chen, Guo-Qing Zhang, Li-Jun Lang, Zhi Li, and Shi-Liang Zhu. Skin superfluid, topological Mott insulators, and asymmetric dynamics in an interacting non-Hermitian Aubry-André-Harper model. *Phys. Rev. B*, 101:235150, Jun 2020.
- [58] Tao Liu, James Jun He, Tsuneya Yoshida, Ze-Liang Xiang, and Franco Nori. Non-Hermitian topological Mott insulators in one-dimensional fermionic superlattices. *Phys. Rev. B*, 102:235151, Dec 2020.

- [59] Zhihao Xu and Shu Chen. Topological Bose-Mott insulators in one-dimensional non-Hermitian superlattices. *Phys. Rev. B*, 102:035153, Jul 2020.
- [60] Ching Hua Lee. Many-body topological and skin states without open boundaries. *Phys. Rev. B*, 104:195102, Nov 2021.
- [61] Faisal Alsallom, Loïc Herviou, Oleg V. Yazyev, and Marta Brzezińska. Fate of the non-Hermitian skin effect in many-body fermionic systems. *Phys. Rev. Res.*, 4:033122, Aug 2022.
- [62] Song-Bo Zhang, M. Michael Denner, Tomáš Bzdušek, Michael A. Sentef, and Titus Neupert. Symmetry breaking and spectral structure of the interacting Hatano-Nelson model. *Phys. Rev. B*, 106:L121102, Sep 2022.
- [63] Kohei Kawabata, Ken Shiozaki, and Shinsei Ryu. Many-body topology of non-Hermitian systems. *Phys. Rev. B*, 105:165137, Apr 2022.
- [64] Tsuneya Yoshida and Yasuhiro Hatsugai. Reduction of one-dimensional non-Hermitian point-gap topology by interactions. *Phys. Rev. B*, 106:205147, Nov 2022.
- [65] W. N. Faugno and Tomoki Ozawa. Interaction-induced non-hermitian topological phases from a dynamical gauge field. *Phys. Rev. Lett.*, 129:180401, Oct 2022.
- [66] Beom Hyun Kim, Jae-Ho Han, and Moon Jip Park. Collective non-hermitian skin effect: point-gap topology and the doublon-holon excitations in non-reciprocal many-body systems. *Communications Physics*, 7(1):73, Mar 2024.
- [67] Shu Hamanaka and Kohei Kawabata. Multifractality of the many-body non-Hermitian skin effect. *Phys. Rev. B*, 111:035144, Jan 2025.
- [68] Ruizhe Shen, Fang Qin, Jean-Yves Desaulles, Zlatko Papić, and Ching Hua Lee. Enhanced Many-Body Quantum Scars from the Non-Hermitian Fock Skin Effect. *Phys. Rev. Lett.*, 133:216601, Nov 2024.
- [69] Kenji Shimomura and Masatoshi Sato. General Criterion for Non-Hermitian Skin Effects and Application: Fock Space Skin Effects in Many-Body Systems. *Phys. Rev. Lett.*, 133:136502, Sep 2024.
- [70] Pietro Brighi and Andreas Nunnenkamp. Nonreciprocal dynamics and the non-Hermitian skin effect of repulsively bound pairs. *Phys. Rev. A*, 110:L020201, Aug 2024.
- [71] Yu-Min Hu, Zijian Wang, Biao Lian, and Zhong Wang. Many-Body Non-Hermitian Skin Effect with Exact Steady States in the Dissipative Quantum Link Model. *Phys. Rev. Lett.*, 135:260401, Dec 2025.
- [72] Pietro Brighi, Marko Ljubotina, Federico Roccati, and Federico Balducci. Finite steady-state current defies non-Hermitian many-body localization. *Phys. Rev. Res.*, 7:L042014, Oct 2025.
- [73] F. Monteiro, T. Micklitz, Masaki Tezuka, and Alexander Altland. Minimal model of many-body localization. *Phys. Rev. Res.*, 3:013023, Jan 2021.
- [74] Giuseppe De Tomasi, Ivan M. Khaymovich, Frank Pollmann, and Simone Warzel. Rare thermal bubbles at the many-body localization transition from the fock space point of view. *Phys. Rev. B*, 104:024202, Jul 2021.
- [75] Naomichi Hatano and David R. Nelson. Localization Transitions in Non-Hermitian Quantum Mechanics. *Phys. Rev. Lett.*, 77:570–573, Jul 1996.
- [76] Naomichi Hatano and David R. Nelson. Vortex pinning and non-Hermitian quantum mechanics. *Phys. Rev. B*, 56:8651–8673, Oct 1997.
- [77] Ryo Okugawa, Ryo Takahashi, and Kazuki Yokomizo. Second-order topological non-hermitian skin effects. *Phys. Rev. B*, 102:241202, Dec 2020.
- [78] Kohei Kawabata, Masatoshi Sato, and Ken Shiozaki. Higher-order non-hermitian skin effect. *Phys. Rev. B*, 102:205118, Nov 2020.

- [79] Hyungwon Kim and David A. Huse. Ballistic Spreading of Entanglement in a Diffusive Nonintegrable System. *Phys. Rev. Lett.*, 111:127205, Sep 2013.
- [80] Leh-Hun Gwa and Herbert Spohn. Six-vertex model, roughened surfaces, and an asymmetric spin Hamiltonian. *Phys. Rev. Lett.*, 68:725–728, Feb 1992.
- [81] Leh-Hun Gwa and Herbert Spohn. Bethe solution for the dynamical-scaling exponent of the noisy Burgers equation. *Phys. Rev. A*, 46:844–854, Jul 1992.
- [82] Doochul Kim. Bethe ansatz solution for crossover scaling functions of the asymmetric XXZ chain and the Kardar-Parisi-Zhang-type growth model. *Phys. Rev. E*, 52:3512–3524, Oct 1995.
- [83] Arnd Bäcker, Masudul Haque, and Ivan M. Khaymovich. Multifractal dimensions for random matrices, chaotic quantum maps, and many-body systems. *Phys. Rev. E*, 100:032117, Sep 2019.
- [84] Kohei Kawabata, Zhenyu Xiao, Tomi Ohtsuki, and Ryuichi Shindou. Singular-Value Statistics of Non-Hermitian Random Matrices and Open Quantum Systems. *PRX Quantum*, 4:040312, Oct 2023.
- [85] Lucas Sá, Pedro Ribeiro, and T. Prosen. Complex Spacing Ratios: A Signature of Dissipative Quantum Chaos. *Phys. Rev. X*, 10:021019, Apr 2020.
- [86] R. Nandkishore and D. A. Huse. Many-Body Localization and Thermalization in Quantum Statistical Mechanics. *Annu. Rev. Condens. Matter Phys.*, 6:15, 2015.
- [87] Dmitry A. Abanin, Ehud Altman, Immanuel Bloch, and Maksym Serbyn. Colloquium: Many-body localization, thermalization, and entanglement. *Rev. Mod. Phys.*, 91:021001, May 2019.
- [88] Zhenyu Xu, Luis Pedro García-Pintos, Aurélia Chenu, and Adolfo del Campo. Extreme Decoherence and Quantum Chaos. *Phys. Rev. Lett.*, 122:014103, Jan 2019.
- [89] Ryusuke Hamazaki, Kohei Kawabata, and Masahito Ueda. Non-Hermitian Many-Body Localization. *Phys. Rev. Lett.*, 123:090603, Aug 2019.
- [90] Sergey Denisov, Tetyana Lapyteva, Wojciech Tarnowski, Dariusz Chruściński, and Karol Życzkowski. Universal Spectra of Random Lindblad Operators. *Phys. Rev. Lett.*, 123:140403, Oct 2019.
- [91] Tankut Can. Random Lindblad dynamics. *J. Phys. A*, 52:485302, 2019.
- [92] Ryusuke Hamazaki, Kohei Kawabata, Naoto Kura, and Masahito Ueda. Universality classes of non-Hermitian random matrices. *Phys. Rev. Research*, 2:023286, Jun 2020.
- [93] Gernot Akemann, Mario Kieburg, Adam Mielke, and T. Prosen. Universal Signature from Integrability to Chaos in Dissipative Open Quantum Systems. *Phys. Rev. Lett.*, 123:254101, Dec 2019.
- [94] Jiachen Li, T. Prosen, and Amos Chan. Spectral Statistics of Non-Hermitian Matrices and Dissipative Quantum Chaos. *Phys. Rev. Lett.*, 127:170602, Oct 2021.
- [95] Antonio M. García-García, Lucas Sá, and Jacobus J. M. Verbaarschot. Symmetry Classification and Universality in Non-Hermitian Many-Body Quantum Chaos by the Sachdev-Ye-Kitaev Model. *Phys. Rev. X*, 12:021040, May 2022.
- [96] Giorgio Cipolloni and Jonah Kudler-Flam. Entanglement Entropy of Non-Hermitian Eigenstates and the Ginibre Ensemble. *Phys. Rev. Lett.*, 130:010401, Jan 2023.
- [97] Lucas Sá, Pedro Ribeiro, and T. Prosen. Symmetry Classification of Many-Body Lindbladians: Tenfold Way and Beyond. *Phys. Rev. X*, 13:031019, Aug 2023.
- [98] Kohei Kawabata, Anish Kulkarni, Jiachen Li, Tokiro Numasawa, and Shinsei Ryu. Symmetry of Open Quantum Systems: Classification of Dissipative Quantum Chaos. *PRX Quantum*, 4:030328, Aug 2023.

- [99] Federico Roccati, Federico Balducci, Ruth Shir, and Aurélie Chenu. Diagnosing non-Hermitian many-body localization and quantum chaos via singular value decomposition. *Phys. Rev. B*, 109:L140201, Apr 2024.
- [100] Shu Hamanaka, Askar A. Iliasov, Titus Neupert, Tomáš Bzdušek, and Tsuneya Yoshida. Multifractal statistics of non-Hermitian skin effect on the Cayley tree. *Phys. Rev. B*, 111:075162, Feb 2025.
- [101] Boris L. Altshuler, Yuval Gefen, Alex Kamenev, and Leonid S. Levitov. Quasiparticle Lifetime in a Finite System: A Nonperturbative Approach. *Phys. Rev. Lett.*, 78:2803–2806, Apr 1997.
- [102] K.S. Tikhonov and A.D. Mirlin. From anderson localization on random regular graphs to many-body localization. *Annals of Physics*, 435:168525, 2021. Special Issue on Localisation 2020.
- [103] Junsong Sun, Chang-An Li, Qingyang Guo, Weixuan Zhang, Shiping Feng, Xiangdong Zhang, Huaiming Guo, and Björn Trauzettel. Non-Hermitian quantum fractals. *Phys. Rev. B*, 110:L201103, Nov 2024.
- [104] Naomichi Hatano, Hosho Katsura, and Kohei Kawabata. Quantum transport on Bethe lattices with non-Hermitian sources and a drain, 2024. arXiv:2409.01873.
- [105] A. Mildenerger, F. Evers, and A. D. Mirlin. Dimensionality dependence of the wave-function statistics at the Anderson transition. *Phys. Rev. B*, 66:033109, Jul 2002.
- [106] K.B. Efetov. Effective medium approximation in the localization theory: Saddle point in a lagrangian formulation. *Physica A: Statistical Mechanics and its Applications*, 167(1):119–131, 1990.
- [107] Yan V. Fyodorov, Alexander D. Mirlin, and Hans-Jürgen Sommers. A novel field theoretical approach to the Anderson localization: sparse random hopping model. *J. Phys. I France*, 2(8):1571–1605, 1992.
- [108] Alexander D. Mirlin and Yan V. Fyodorov. Distribution of local densities of states, order parameter function, and critical behavior near the Anderson transition. *Phys. Rev. Lett.*, 72:526–529, Jan 1994.
- [109] Alexander D. Mirlin and Yan V. Fyodorov. Statistical properties of one-point Green functions in disordered systems and critical behavior near the Anderson transition. *J. Phys. I France*, 4(5):655–673, 1994.
- [110] A. De Luca, B. L. Altshuler, V. E. Kravtsov, and A. Scardicchio. Anderson Localization on the Bethe Lattice: Nonergodicity of Extended States. *Phys. Rev. Lett.*, 113:046806, Jul 2014.
- [111] Claudio de C. Chamon, Christopher Mudry, and Xiao-Gang Wen. Localization in Two Dimensions, Gaussian Field Theories, and Multifractality. *Phys. Rev. Lett.*, 77:4194–4197, Nov 1996.
- [112] Alexander D. Mirlin, Yan V. Fyodorov, Frank-Michael Dittes, Javier Quezada, and Thomas H. Seligman. Transition from localized to extended eigenstates in the ensemble of power-law random banded matrices. *Phys. Rev. E*, 54:3221–3230, Oct 1996.
- [113] Norbert Rosenzweig and Charles E. Porter. "Repulsion of Energy Levels" in Complex Atomic Spectra. *Phys. Rev.*, 120:1698–1714, Dec 1960.
- [114] Giuseppe De Tomasi and Ivan M. Khaymovich. Non-Hermitian Rosenzweig-Porter random-matrix ensemble: Obstruction to the fractal phase. *Phys. Rev. B*, 106:094204, Sep 2022.
- [115] Cem Yuce. Nonlinear non-Hermitian skin effect. *Physics Letters A*, 408:127484, 2021.
- [116] Motohiko Ezawa. Dynamical nonlinear higher-order non-Hermitian skin effects and topological trap-skin phase. *Phys. Rev. B*, 105:125421, Mar 2022.
- [117] C. Yuce. Nonlinear skin modes and fixed points. *Phys. Rev. B*, 111:054201, Feb 2025.

- [118] Stefano Longhi. Modulational Instability and Dynamical Growth Blockade in the Nonlinear Hatano–Nelson Model. *Advanced Physics Research*, 4(5):2400154, 2025.
- [119] Kohei Kawabata and Daichi Nakamura. Hopf Bifurcation of Nonlinear Non-Hermitian Skin Effect. *Phys. Rev. Lett.*, 135:126610, Sep 2025.
- [120] Shu Hamanaka. Koopman Nonlinear Non-Hermitian Skin Effect, 2026. arXiv:2601.03636.